Multivalency effects of hemagglutinin component of type B botulinum neurotoxin complex on epithelial barrier disruption

Multivalency effects of hemagglutinin component of type B botulinum neurotoxin complex on epithelial barrier disruption

Sho Amatsu, Takuhiro Matsumura, Masahiro Yutani, and Yukako Fujinaga*

Department of Bacteriology, Graduate School of Medical Sciences, Kanazawa University, Ishikawa, Japan.

* Correspondence: Yukako Fujinaga, Department of Bacteriology, Graduate School of Medical Sciences, Kanazawa University, Ishikawa, Japan.

Tel: +81-76-265-2200, Fax: +81-76-234-4230

Email**:** yukafuji@med.kanazawa-u.ac.jp

Short running title: Multivalency effect of HA

Original Articles

Subject Section: Bacteriology, **Specified Field:** Toxin

Abstract

Hemagglutinin (HA) is one of the components of botulinum neurotoxin (BoNT) complexes and it promotes the absorption of BoNT through the intestinal epithelium by at least two specific mechanisms: cell surface attachment by carbohydrate binding, and epithelial barrier disruption by E-cadherin binding. It is known that HA forms a three-arm structure, in which each of three protomers has three carbohydrate-binding sites and one E-cadherin-binding site. A three-arm form of HA is considered to bind to these ligands simultaneously. In this study, we investigated how the multivalency effect of HA influences its barrier-disrupting activity. We prepared type B full-length HA (three-arm form) and mini-HA, which is a deletion mutant lacking the trimer-forming domain. Size-exclusion chromatography analysis showed that mini-HA exists as dimers (two-arm form) and monomers (one-arm form), which are then separated. We examined the multivalency effect of HA on the barrier-disrupting activity, the E-cadherin-binding activity, and the attachment activity to the basolateral cell surface. Our results showed that HA initially attaches to the basal surface of Caco-2 cells by carbohydrate binding and then moves to the lateral cell surface, where the HA acts to disrupt the epithelial barrier. Our results demonstrated that the multivalency effect of HA enhances the barrier-disrupting activity in Caco-2 cells. We found that the basal cell surface attachment and binding ability to immobilized E-cadherin were enhanced by the multivalency effect of HA. These results suggest that at least these two factors induced by the multivalency effect of HA cause the enhancement of the barrier-disrupting activity.

Keywords

botulinum neurotoxin, epithelial barrier, hemagglutinin, multivalent binding

Introduction

Botulinum neurotoxin (BoNT) is one of the food-poisoning agents and the most potent bacterial toxin. BoNTs have been classified serologically into serotype A to G, and these toxins cleave soluble *N*-ethylmaleimide-sensitive factor attachment protein receptor (SNARE) proteins in peripheral nerve terminals, resulting in the blocking of neurotransmitter release (1). Serotypes A, B, E, and F cause human botulism, whereas serotypes C and D mainly cause animal botulism (2). BoNTs are produced as progenitor toxin complexes (PTCs) with neurotoxin-associated proteins (NAPs), which include non-toxic non-hemagglutinin (NTNHA) and hemagglutinin (HA). The oral toxicity of BoNTs is markedly increased in association with NAPs, and the larger forms of PTCs, the greater its oral toxicity (3). There are three forms of PTC: M-PTC, L-PTC, and LL-PTC (also known as 12S toxin, 16S toxin, and 19S toxin, respectively) (3, 4). M-PTC consists of BoNT and NTNHA, and L-PTC consists of BoNT, NTNHA, and HA (Fig. 1a). LL-PTC is assumed to be a dimer of L-PTC (5). When assembled into PTCs, NTNHA protects BoNT from an acidic pH and proteolytic enzymes in the gastrointestinal tract (6, 7). HA facilitates BoNT absorption across the intestinal epithelium by at least two specific mechanisms: the attachment to the luminal surface of the intestinal epithelial cells by carbohydrate binding (8–14), and the epithelial barrier disruption by E-cadherin binding (15–19). We have proposed an HA-mediated three-step mechanism for the intestinal absorption of L-PTC (20). In the first step, L-PTC binds to glycoproteins/glycolipids at the luminal surface of the intestinal epithelial cells, followed by transcytosis. Then, the HA component of L-PTC delivered to the basolateral side of epithelial cells directly binds to E-cadherin, which exclusively resides on the basolateral surface of epithelial cells, leading to epithelial barrier

disruption. Finally, the disruption allows PTCs to pass through the paracellular route (20).

HA is composed of three subcomponents: HA1, HA2, and HA3 (also known as HA33, HA17, and HA70, respectively) (21). Six HA1, three HA2, and three HA3 are assembled into a triskelion-shaped hetero-dodecamer in which homo-trimeric HA3 forms the core of the complex (Fig. 1a,b) (22–25). Hence, the triskelion-shaped HA is a trimer of three protomers, composed of two HA1, one HA2, and one HA3, and it has a "three-arm" structure (Fig. 1a,b). The carbohydrate-binding activity of HA is attributable to HA1 and HA3, which binds to galactose and sialic acid, respectively (9). In addition, HA1s of types C and D also bind to sialic acid (10, 26). Triskelion-shaped HAs of types A and B have six galactose-binding sites and three sialic acid-binding sites (23–25). HAs of types A and B bind to E-cadherin; a region extending over HA2 and the C-terminal domain of HA3 interacts with E-cadherin ectodomain 1-2 (EC1-2) (17–19). Lee, *et al.* reported that, using isothermal titration calorimetry (ITC), HA (full-length HA, FL-HA) of type A interacts with E-cadherin EC1-2 expressed in *Escherichia coli* with a dissociation constant (K_d) ~2.3 μM and a 1:3 HA-E-cadherin stoichiometry (18). It was also reported that a truncated mutant of HA (termed mini-HA) of type A, which lacks the trimer-forming domain of HA3 and represents "one-arm" of the HA, interacts with EC1-2 with a K_d ~2.7 μM and a 1:1 HA-E-cadherin stoichiometry (18).

Carbohydrate-binding sites and E-cadherin-binding sites are located within each arm of HA (Fig. 1c) (18, 19, 24). Therefore, triskelion-shaped HA is capable of exerting multivalent binding to these ligands. In this study, we prepared type B FL-HA; three-arm HA, dimers of mini-HA; two-arm HA, and monomers of mini-HA; one-arm HA, and we investigated the multivalency effects of HA on the epithelial barrier disruption.

Materials and Methods

Plasmid construction

The genomic DNA was extracted and purified from *C. botulinum* type B strain Okra. HA1 (aa 7-294) encoding gene was cloned into the *Kpn*I-*Sal*I site of the pET52b(+) vector (Novagen, Merck Millipore, Madison, WI, USA), and an oligonucleotide encoding a FLAG-tag was inserted at the C-terminus of HA1. HA2 (aa 2-146) encoding gene was cloned into the *Hin*dIII-*Kpn*I site of pT7-FLAG-1 vector (Sigma Aldrich, St. Louis, MO, USA). The full-length HA3 (HA3-FL, aa 19-626) encoding gene was cloned into the *Kpn*I-*Sal*I site of the pET52b(+) vector. The truncated mutant of HA3 (termed HA3-mini, aa 380-626) encoding gene was cloned into the *Nco*I-*Sal*I site of the pET52b(+) vector, and an oligonucleotide encoding a *Strep*-tag II tag was inserted at the C-terminus of HA3-mini. Site-directed mutagenesis was performed using PrimeSTAR Max polymerase (Takara Bio, Shiga, Japan). The inserted regions of these plasmids and the presence of mutation were confirmed by DNA sequencing.

Protein expression and purification

The expression of HA proteins was conducted using Overnight Express Autoinduction System 1 (Novagen, Merck Millipore, Darmstadt, Germany), as previously described (25). FLAG-tagged proteins, HA1 with a C-terminal FLAG-tag (HA1-FLAG) and HA2 with an N-terminal FLAG-tag (FLAG-HA2), were purified using anti-FLAG tag M2 agarose gel beads (Sigma Aldrich, St. Louis, MO, USA). *Strep*-tag II-tagged proteins, HA3-FL with an N-terminal *Strep*-tag II tag (*Strep*-HA3-FL) and HA3-mini with a C-terminal *Strep*-tag II tag (HA3-mini-*Strep*), were purified

using StrepTrap HP (GE Healthcare, Freiburg, Germany). All proteins were dialyzed against PBS (pH 7.4).

Recombinant mouse E-cadherin ectodomain 1-5 protein with a hexa-histidine tag at the C-terminus (E-cadherin EC1-5-His) was expressed in HEK293 cells, and purified as previously described (17).

In vitro reconstitution and purification of HAs

The purified HA1, HA2, and HA3 (HA3-FL for FL-HA, HA3-mini for mini-HA) were mixed at a molar ratio of 4:4:1 in PBS and incubated for 3 hr at 37°C. The FL-HA and mini-HA complexes were purified using StrepTrap HP. The mini-HA complex was subjected to further purification on a Superdex 200 Increase 10/300 GL column (GE Healthcare, Uppsala, Sweden) in PBS. Purified proteins were dialyzed against PBS.

Size-exclusion chromatography analysis of HAs

Fifty μg of each purified HA protein was loaded onto a Superdex 200 Increase 10/300 GL column in PBS. Twenty-five μg of each mini-HA (in a concentration of 2.2 μM as protomers) was incubated at 37°C for the indicated time. Then, the mini-HA was loaded onto a Superdex 200 Increase 10/300 GL column in PBS. The protein concentration of the elution was measured based on absorbance at 280 nm.

Transepithelial electrical resistance (TER) assay

Measurement of TER was performed using Millicell-ERS (Merck Millipore, Billerica, MA, USA), as previously described (15). In brief, Caco-2 cells were grown on 24-well collagen-coated Transwell filters (Corning, Tewksbury, MA, USA) in Eagle's MEM (Gibco, ThermoFisher Scientific, Ghent, Belgium) supplemented with 20% fatal bovine

serum (FBS) until completely confluent, and Caco-2 cell monolayers were formed. HAs were added to the basolateral side of the monolayers at final concentrations of 51 nM of protomer of HAs (17 nM FL-HA; 25.5 nM dimer fraction of mini-HA; 51 nM monomer fraction of mini-HA), 102 nM of protomer of a dimer fraction of mini-HA (51 nM dimer fraction), and 255 nM of protomer of a monomer fraction of mini-HA (255 nM monomer fraction). TER was measured at time points up to 24 hr post-addition.

Pull-down assay

FL-HAs and mini-HAs (20 pmol of protomer of HAs) were immobilized onto Strep-Tactin Superflow agarose gel beads (Novagen, Merck Millipore, Darmstadt, Germany) by incubation for 1 hr at 4°C in TNCX buffer (50 mM Tris-HCl pH 7.4, 150 mM NaCl, 2 mM $CaCl_2$, 0.01% Triton X-100). The concentration of E-cadherin ectodomain protein was adjusted to 100 nM in TNCX buffer. A 200 µl aliquot of E-cadherin solution was subjected to pull-down with beads coupled to FL-HA, a dimer fraction or a monomer fraction of mini-HA for 2 hr at 4°C. The beads were washed three times, and the bound proteins were eluted in SDS-PAGE sample buffer. Samples were separated by 12.5% SDS-PAGE and transferred to a PVDF membrane (Immobilon-P; Merck Millipore, Darmstadt, Germany), followed by immunoblotting with rat anti-mouse E-cadherin monoclonal antibody (ECCD-2; Takara Bio, Shiga, Japan; 1:500). Bound antibodies were probed with horseradish-peroxidase (HRP)-conjugated goat anti-rat IgG antibody (Jackson ImmunoResearch, West Grove, PA, USA; 1:10000), and the membranes were developed using ECL select (Amersham, GE Healthcare, Buckinghamshire, UK). After immunoblotting, the membranes were stained with Coomassie brilliant blue (CBB) to visualize HA proteins.

Sandwich enzyme linked immunosorbent assay (ELISA)

Ninety-six-well microtiter plates (IWAKI, Tokyo, Japan) were coated with 100 μl of mouse anti-His tag antibody (OGHis; MBL, Nagoya, Japan; 1:1000) in 0.05 M carbonate buffer at pH 9.6. Subsequent incubations were carried out for 1 hr at 37°C. After washing with TNCT buffer (50 mM Tris-HCl pH 7.4, 150 mM NaCl, 2 mM $CaCl_2$, 0.05% Tween-20), plates were blocked with 1% BSA in TNCT buffer. Plates were washed and incubated with 100 nM E-cadherin EC1-5-His in the blocking buffer (1% BSA in TNCT buffer). Then, plates were washed and incubated with 100 nM of protomer of HAs. After washing, plates were incubated with rabbit anti-FLAG tag polyclonal antibody (#2368; Cell Signaling Technology, Beverly, MA, USA; 1:1000) in the blocking buffer, followed by HRP-conjugated goat anti-rabbit IgG antibody (Jackson ImmunoResearch, West Grove, PA, USA; 1:10000). Plates were developed using ABTS (Roche Diagnostics, Mannheim, Germany), and the absorbance at 405 nm was read.

Cell-ELISA

Caco-2 cells were grown on 24-well collagen-coated Transwell filters until completely confluent. HAs were added to the basolateral side at a final concentration of 51 nM protomer, and the monolayers were incubated in Caco-2 cell culture medium (MEM, 20% FBS) for 40 min at 4°C. After washing with ice-cold PBS, the cells on the Transwell filters were fixed with 4% paraformaldehyde (PFA) for 30 min at 4°C, followed by blocking with 5% BSA in PBS for 30 min at room temperature. Then, the basolateral sides of the monolayers were incubated with mouse anti-FLAG tag monoclonal antibody (M2; Sigma Aldrich, St. Louis, MO, USA; 1:5000) in the

blocking buffer (5% BSA in PBS) for 2 hr at 37°C, followed by HRP-conjugated donkey anti-mouse IgG antibody (Jackson ImmunoResearch, West Grove, PA, USA; 1:10000) for 1 hr at 37°C. The Transwell filters were developed using ABTS, and the absorbance at 405 nm was read.

Immunofluorescence

HAs were added to the basolateral side of Caco-2 cells grown on Transwell filters, and the monolayers were incubated in the Caco-2 cell culture medium for 40 min at 4°C. After fixation with 4% PFA for 30 min at 4°C and permeabilization with 0.5% Triton X-100 in PBS for 5 min at room temperature, the cells were blocked with 5% BSA in PBS for 30 min at room temperature. Then, HA was stained with a mouse anti-FLAG tag (1:1000) monoclonal antibody, followed by Cy3-conjugated donkey anti-mouse IgG antibody (Jackson ImmunoResearch, West Grove, PA, USA; 1:400). After immunostaining, the Transwell filters were mounted in ProLong antifade reagent (Molecular Probes, ThermoFisher Scientific, Eugene, OR, USA). Images were acquired by confocal microscopy using a CSUX1 confocal scanner unit (Yokogawa Electric, Tokyo, Japan) and IX71 microscope (Olympus, Tokyo, Japan) and processed using Metamorph software (Molecular Devices, Sunnyvale, CA, USA).

Pulse-chase analysis

The purified FLAG-HA2 was labeled using Alexa Fluor 568-NHS (Molecular Probes, ThermoFisher Scientific, Eugene, OR, USA) following the manufacturer's protocol. Alexa-labeled HA complexes were reconstituted from Alexa-labeled FLAG-HA2 and non-labeled HA1-FLAG and HA3 (*Strep*-HA3-FL for FL-HA, HA3-mini-*Strep* for

mini-HA), and purified as described in the *In vitro* reconstitution and purification of HAs section. The SEC profiles of Alexa-labeled HA complexes are consistent with those of non-labeled HA complexes (data not shown). Basolateral sides of Caco-2 cells grown on collagen-coated 24-well Transwell filters were incubated with 153 nM of protomer of Alexa-labeled HA complexes in the Caco-2 cell culture medium for 40 min at 4°C. After a brief wash in the ice-cold Caco-2 cell culture medium, the monolayers were incubated with 153 nM protomer of non-labeled HA complexes in the Caco-2 cell culture medium for the indicated time (10 or 20 min) at 37°C. After pulse or chase labeling, the monolayers were fixed and stained with rat anti-E-cadherin (DECMA-1; Sigma-Aldrich, St. Louis, MO, USA; 1:1000) and mouse anti-ZO-1 (ZO1-1A12; Zymed, ThermoFisher Scientific, Carlsbad, CA, USA; 1:250) monoclonal antibodies, followed by Alexa Fluor 488-conjugated goat anti-rat IgG antibody (Molecular Probes, ThermoFisher Scientific, Eugene, OR, USA; 1:400) and Alexa Fluor 405-conjugated goat anti-mouse IgG antibody (Molecular Probes, ThermoFisher Scientific, Eugene, OR, USA; 1:400), respectively. After immunostaining, images were acquired by confocal microscopy.

Results

Preparation of one-, two-, and three-arm HAs

Full-length HAs (FL-HAs) and mini-HAs of type B were reconstituted *in vitro* from purified HA subcomponents expressed in *E. coli* (Fig. 2 and Supp. Fig. 1a). We constructed the mini-HA of type B, which consists of HA1, HA2, and an HA3 mutant deleted N-terminal 379 amino acid (aa) residues, in the same manner as mini-HA of type A reported by Lee *et al.* (24). Reconstituted mini-HA showed two major peaks by size-exclusion chromatography (SEC) (Fig. 2a). Among all HA subcomponents, only HA3-mini showed the two similar peaks (Supp. Fig. 1a). It is considered that the dimerization of mini-HA is due to a weak association between HA3-minis. After SEC separation of the two major peaks of mini-HA, the re-run profiles of each fraction on SEC showed single major peaks individually at 10.5 ml (dimer, corresponding to two-arm HA, predicted mass: 232 kDa) and 12.5 ml (monomer, corresponding to one-arm HA, predicted mass: 116 kDa) (Fig. 2b). While the height of each minor peak of mini-HAs was slightly increased after incubation at 37°C for 24 hr in PBS, each major peak was mostly retained (Supp. Fig. 1b,c). FL-HA was predominantly eluted at 9.0 ml (corresponding to three-arm HA, predicted mass: 474 kDa) in SEC (Fig. 2b).

Fractionated mini-HAs disrupt the epithelial barrier of Caco-2 cells

In polarized epithelial cells, junctional complexes such as tight junctions (TJs), E-cadherin-based adherence junctions (AJs), and desmosomes are oriented in an apical-to-basal arrangement (27). Epithelial TJs seal adjacent epithelial cells and regulate the paracellular permeability (28). Thus, macromolecules, *e.g.*, HA and PTCs, do not gain

direct access to E-cadherin from the apical side of the epithelial cell, suggesting that a transcytosis step to the basolateral side is required for apically applied HA to interact with E-cadherin (15). To assess the direct barrier-disrupting activities of HAs, we measured the transepithelial electrical resistance (TER) of Caco-2 cell monolayers following basolateral treatment with HAs (Fig. 3). FL-HA and dimer and monomer fractions of mini-HA disrupted the epithelial barrier of Caco-2 cells (Fig. 3). The barrier-disrupting activities of dimer and monomer fractions of mini-HA were decreased to approximately one-half and one-fifth of that of FL-HA, respectively (Fig. 3). The TER value of Caco-2 cells with FL-HA was decreased to 84% at 2 hr post addition, and that with the higher concentration of dimer (102 nM as protomer, 2x Dimer) and monomer (255 nM, 5x Monomer) fractions of mini-HA was decreased to 54 and 69%, respectively (Fig. 3). However, the TER values after 6 hr post addition with mini-HAs (2x Dimer. 41~30%; 5x Monomer, 46~41%) was higher than that of FL-HA (37~17%) (Fig. 3).

Binding of HAs to E-cadherin

To assess the interaction between HAs and the E-cadherin extracelluar domain, we performed pull-down assays and sandwich ELISAs using recombinant E-cadherin EC1-5-His, which was expressed in HEK293 cells and purified (Fig. 4). In the pull-down assay, E-cadherin EC1-5 comparably bound to *Strep*-tag II tagged FL-HA wild-type (WT) and mini-HAs immobilized on Strep-Tactin beads (Fig. 4a). In the sandwich ELISA, E-cadherin EC1-5, which contains a hexa-histidine tag at the C-terminus, was immobilized to anti-His tag antibody-coated plates, and then HAs were added to these plates. As a result, the E-cadherin-binding abilities of dimer and monomer fractions of

mini-HA were relatively weak, and 65% and 10% of that of FL-HA WT, respectively (Fig. 4b). It has been reported that HA3 Lys607 is located at the interface with E-cadherin (Fig. 1c), and its alanine substitution (K607A, KA) impairs the E-cadherin-binding and barrier-disrupting activity (18, 19). FL-HA harboring a KA mutation (FL-HA^{KA}) did not interact with E-cadherin EC1-5 in these experiments (Fig. 4).

Attachments of HAs to the basolateral surface of Caco-2 cells

We examined the abilities of HAs to attach to the basolateral cell surface by cell-ELISA using Caco-2 cell monolayers (Fig. 5a). FL-HA WT attached to the basolateral cell surface (Fig. 5a). To identify how HA attaches to the basolateral surface of Caco-2 cells, we performed these experiments using functional mutants of FL-HA. The galactose-binding site of HA1 and the sialic acid-binding site of HA3 have already been identified in type A, B, and C by co-crystallization with saccharides (Fig. 1c) (24, 29–31). It has also been reported that alanine substitutions of HA1 Asn286 (N286A, NA) and HA3 Arg528 (R528A, RA) abolish each carbohydrate binding (19, 24, 29). FL-HA WT attached to the basolateral cell surface (Fig. 5a). FL-HA harboring an NA mutation (FL-HA^{NA}) rarely attached to the basolateral cell surface (Fig. 5a). The basolateral cell surface attachment of FL-HA harboring an RA mutation (FL-HA^{RA}) was 70% of that of FL-HA WT, and that of FL-HA^{KA} was comparable with that of FL-HA WT (Fig. 5a). These results indicate that HA attached to the basolateral surface of Caco-2 cells by binding mainly to galactose. The basolateral cell surface attachment of dimer and monomer fractions of mini-HA were 20% and 7% of that of FL-HA WT, respectively (Fig. 5a). Next, HAs that attached to the basal cell surface were visualized using immunofluorescence (Fig. 5b). FL-HA WT, FL-HA^{RA}, and FL-HA^{KA} attached to the

basal surface of Caco-2 cells homogeneously (Fig. 5b). The FL-HA^{NA} attached to the cell surface was rarely observed (Fig. 5b). The attachment of the dimer fraction of mini-HA to the basal cell surface was weaker than FL-HA WT, and the monomer fraction of mini-HA showed very weak attachment (Fig. 5b).

Pulse-chase analysis

The z-stacked images showed that basolaterally applied HAs localized only to the basal cell surface, and not to the lateral cell surface at 4°C (Fig. 6a). It has been reported that basolaterally applied FL-HA WT localized to the basal and lateral surfaces of Caco-2 cells when incubated continuously at 37°C (17, 19). Therefore, we postulate that HA attaching to the basal cell surface moves to the lateral cell surface. To examine this hypothesis, we performed pulse-chase experiments (Fig. 6a-c). After chasing for 10 ~ 20 min at 37°C, some of the FL-HA WT that attached to the basal cell surface moved to the lateral cell surface (Fig. 6b,c). In the similar way, the dimer fraction of mini-HA moved to the lateral cell surface, albeit at a lower level compared with FL-HA WT. The monomer fraction of mini-HA moved to the lateral cell surface only slightly (Fig. 6c). FL-HA^{KA} did not localize to the lateral cell surface, and some of the FL-HA^{KA} were endocytosed into the cytoplasm (Fig. 6b,c). E-cadherin showed major localization throughout the lateral cell surface and infrequent localization to the basal cell surface (Fig. 6a,b).

Discussion

Our results showed that the greater number of arms HA has, the more effectively it disrupts the epithelial barrier of human intestinal Caco-2 cell monolayers, that is, the barrier-disrupting activity of HA is markedly increased by the multivalency effect of HA. Our results also revealed that the three-arm form of HA is not essential for epithelial barrier disruption. The monomer fraction of mini-HA slightly compromised the integrity of the epithelial barrier, but significantly compromised it at a higher concentration (Fig. 3). These results imply that one-arm HA is capable of disrupting the epithelial barrier. However, the possibility cannot be excluded that one-arm HA has no activity to disrupt the epithelial barrier, and a small amount of two-arm HA existing in the monomer fraction causes this activity; there might exist dimers of mini-HA in the monomer fraction for some reasons, *e.g.*, contamination of dimers in the fractionation procedure, and/or dimerization under the experimental conditions. The barrier-disrupting activities of mini-HAs are weakened at 4-6 hr post-addition, possibly through the instability of mini-HAs because of the truncating mutation.

Consistent with the results of Lee, *et al.* (18), the binding ability to un-immobilized E-cadherin was comparable between FL-HA and mini-HAs (Fig. 4a). However, the binding ability of HA to immobilized E-cadherin was markedly enhanced by the multivalency effect (Fig. 4b). Assuming that the immobilized E-cadherin exists as a cluster on the plates, these results suggest that the multivalency effect of HA might cause the effective interaction with E-cadherin that resides on the lateral cell surface and exists as a cluster.

We previously found that the barrier-disrupting activity of FL-HA^{NA} was one-fifth of that of FL-HA WT, and the activity of FL-HA^{RA} was slightly less than that of FL-HA

WT, when these HAs were applied from the basolateral side, even though they showed the same binding ability to E-cadherin in the pull-down assay (19). Hence, it is considered that the carbohydrate-binding activity of HA increases the opportunities to meet E-cadherin by promoting the basolateral cell surface attachment, leading to more effective barrier disruption (19). Our present results show that HA attaches to the basal surface of Caco-2 cells by binding mainly to the terminal galactose residue on glycoproteins/glycolipids (Fig. 5 and Fig. 6a). It is well-known that the interaction between carbohydrates and lectins could be markedly enhanced by the multivalency effects of lectins (32–34). In a similar way, the intermediate L-PTC of type D, which has a smaller number of HA1-HA2 complexes than mature L-PTC, attaches to the surface of rat intestinal epithelial IEC-6 cells by carbohydrate binding weaker than mature L-PTC (35). Consistently, our results revealed that the attachment of HA to the basolateral surface of Caco-2 cells is markedly enhanced by the multivalency effect of HA (Fig. 5).

Pulse-chase experiments revealed that basolaterally applied HAs initially attach only to the basal surface of Caco-2 cells, and then the bound HAs move to the lateral cell surface (Fig. 6a-c). FL-HA^{KA}, which does not interact with E-cadherin, was able to attach to the basal cell surface as well as FL-HA WT (Figs. 5 and Fig. 6a). However, FL-HA^{KA} did not move to the lateral cell surface after chasing (Fig. 6b,c). These results suggest that this movement of HA is dictated by E-cadherin. It is known that cadherin molecules flow within the lateral plasma membrane in a basal-to-apical direction and this flow is called “cadherin flow” (36, 37). Therefore, it is assumed that HA binds to E-cadherin at the basal cell surface and then rides on cadherin flow. This movement of HA was increased by the multivalency effect of HA (Fig. 6c). We previously reported that

the amount of the carbohydrate-binding defective mutant FL-HA (FL-HA$^{NA/RA}$, FL-HA harboring both NA and RA) located at the lateral cell surface is much lower than that of FL-HA WT, when these HAs are applied basolaterally and the monolayers are incubated continuously at 37°C (19). These observations indicate that the movement of HA from the basal to lateral cell surface is promoted by the basal cell surface attachment via carbohydrate residues, which consequently increases the opportunities to meet E-cadherin, and this attachment step is enhanced by the multivalency effect of HA.

Recently, we reported that L-PTC of type A enters the host through M cells via GPI-anchored glycoproteins-mediated transcytosis. Binding to these glycoproteins is responsible for HA in a carbohydrate-binding-dependent manner (13). Therefore, it is assumed that the multivalency effect of HA enhances the attachment of L-PTC to the luminal surface of M-cells and increaces the efficiency of transcytosis across the intestinal lumen.

In conclusion, we revealed that basolaterally applied HA initially binds to glycoproteins/glycolipids only at the basal cell surface and then moves to the lateral cell surface, where HA acts to disrupt the epithelial barrier. Our results show that the multivalency effect of HA increases the epithelial barrier-disrupting activity, and this phenomenon is considered to be induced by at least two mechanisms: enhancing the cell surface attachment via carbohydrate residues at the basal cell surface, and enhancing the binding avidity to clustered E-cadherin that resides on the lateral cell surface.

Acknowledgements

We thank Masatoshi Takeichi and Yoshikazu Tsukasaki (RIKEN, CDB) for the generous gifts of E-cadherin-expressing plasmid and cells, and Sachiyo Akagi for technical assistance. This work was partly supported by a Grant-in-Aid for JSPS Research Fellow to S.A. (15J03770) and the project "Development of cell manufacturing and processing system for industrialization of regenerative medicine" from the Japan Agency for Medical Research and Development (AMED) to Y.F. (P14006).

Disclosure

The authors declare no conflicts of interest.

References

1. Schiavo G., Matteoli M., Montecucco C. (2000) Neurotoxins affecting neuroexocytosis. *Physiol Rev* **80**: 717–766.
2. Arnon S.S., Schechter R., Inglesby T.V., Henderson D.A., Bartlett J.G., Ascher M.S., Eitzen E., Fine A.D., Hauer J., Layton M., Lillibridge S., Osterholm M.T., O'Toole T., Parker G., Perl T.M., Russell P.K., Swerdlow D.L., Tonat K. (2001) Botulinum Toxin as a Biological Weapon: Medical and Public Health Management. *JAMA* **285**: 1059–70.
3. Sakaguchi G. (1982) Clostridium botulinum toxins. *Pharmacol Ther* **19**: 165–194.

4. Oguma K., Inoue K., Fujinaga Y., Yokota K., Watanabe T., Ohyama T., Takeshi K., Inoue K. (1999) Structure and Function of Clostridium Botulinum Progenitor Toxin. *J Toxicol* **18**: 17–34.

5. Inoue K., Fujinaga Y., Watanabe T., Ohyama T., Takeshi K., Moriishi K., Nakajima H., Inoue K., Oguma K. (1996) Molecular composition of Clostridium botulinum type A progenitor toxins. *Infect Immun* **64**: 1589–94.

6. Sugii S., Ohishi I., Sakaguchi G. (1977) Correlation between oral toxicity and in vitro stability of Clostridium botulinum type A and B toxins of different molecular sizes. *Infect Immun* **16**: 910–14.

7. Gu S., Rumpel S., Zhou J., Strotmeier J., Bigalke H., Perry K., Shoemaker C.B., Rummel A., Jin R. (2012) Botulinum neurotoxin is shielded by NTNHA in an interlocked complex. *Science* **335**: 977–981.

8. Fujinaga Y., Inoue K., Watanabe S., Yokota K., Hirai Y., Nagamachi E., Oguma K. (1997) The haemagglutinin of Clostridium botulinum type C progenitor toxin plays an essential role in binding of toxin to the epithelial cells of guinea pig small intestine, leading to the efficient absorption of the toxin. *Microbiology* **143**: 3841–3847.

9. Fujinaga Y., Inoue K., Nomura T., Sasaki J., Marvaud J.C., Popoff M.R., Kozaki S., Oguma K. (2000) Identification and characterization of functional subunits of Clostridium botulinum type A progenitor toxin involved in binding to intestinal microvilli and erythrocytes. *FEBS Lett* **467**: 179–183.

10. Fujinaga Y., Inoue K., Watarai S., Sakaguchi Y., Arimitsu H., Lee J.C., Jin Y., Matsumura T., Kabumoto Y., Watanabe T., Ohyama T., Nishikawa A., Oguma K. (2004) Molecular characterization of binding subcomponents of Clostridium

botulinum type C progenitor toxin for intestinal epithelial cells and erythrocytes. *Microbiology* **150**: 1529–38.

11. Arimitsu H., Sakaguchi Y., Lee J.C., Ochi S., Tsukamoto K., Yamamoto Y., Ma S., Tsuji T., Oguma K. (2008) Molecular properties of each subcomponent in Clostridium botulinum type B haemagglutinin complex. *Microb Pathog* **45**: 142–49.
12. Yao G., Lee K., Gu S., Lam K.H., Jin R. (2014) Botulinum Neurotoxin A Complex Recognizes Host Carbohydrates through Its Hemagglutinin Component. *Toxins* **6**: 624–35.
13. Matsumura T., Sugawara Y., Yutani M., Amatsu S., Yagita H., Kohda T., Fukuoka S.I., Nakamura Y., Fukuda S., Hase K., Ohno H., Fujinaga Y. (2015) Botulinum toxin A complex exploits intestinal M cells to enter the host and exert neurotoxicity. *Nat Commun* **6**: 6255.
14. Lam T.I., Stanker L.H., Lee K., Jin R., Cheng L.W. (2015) Translocation of botulinum neurotoxin serotype A and associated proteins across the intestinal epithelia. *Cell Microbiol* **17**: 1133–43.
15. Matsumura T., Jin Y., Kabumoto Y., Takegahara Y., Oguma K., Lencer W.I., Fujinaga Y. (2008) The HA proteins of botulinum toxin disrupt intestinal epithelial intercellular junctions to increase toxin absorption. *Cell Microbiol* **10**: 355–64.
16. Jin Y., Takegahara Y., Sugawara Y., Matsumura T., Fujinaga Y. (2009) Disruption of the epithelial barrier by botulinum haemagglutinin (HA) proteins - differences in cell tropism and the mechanism of action between HA proteins of types A or B, and HA proteins of type C. *Microbiology* **155**: 35–45.
17. Sugawara Y., Matsumura T., Takegahara Y., Jin Y., Tsukasaki Y., Takeichi M.,

Fujinaga Y. (2010) Botulinum hemagglutinin disrupts the intercellular epithelial barrier by directly binding E-cadherin. *J Cell Biol* **189**: 691–700.

18. Lee K., Zhong X., Gu S., Kruel A.M., Dorner M.B., Perry K., Rummel A., Dong M., Jin R. (2014) Molecular basis for disruption of E-cadherin adhesion by botulinum neurotoxin A complex. *Science* **344**: 1405–10.
19. Sugawara Y., Yutani M., Amatsu S., Matsumura T., Fujinaga Y. (2014) Functional Dissection of the Clostridium botulinum Type B Hemagglutinin Complex: Identification of the Carbohydrate and E-Cadherin Binding Sites. *PLoS One* **9**: e111170.
20. Fujinaga Y., Sugawara Y., Matsumura T. (2013) Uptake of Botulinum Neurotoxin in the Intestine. *Curr Top Microbiol Immunol* **364**: 45–59.
21. Fujinaga Y., Inoue K., Shimazaki S., Tomochika K., Tsuzuki K., Fujii N., Watanabe T., Ohyama T., Takeshi K., Inoue K., Oguma K. (1994) Molcular construction of Clostridium botulinum type C progenitor toxin and its gene organization. *Biochem Biophys Res Commun* **205**: 1291–98.
22. Hasegawa K., Watanabe T., Suzuki T., Yamano A., Oikawa T., Sato Y., Kouguchi H., Yoneyama T., Niwa K., Ikeda T., Ohyama T. (2007) A Novel Subunit Structure of *Clostridium botulinum* Serotype D Toxin Complex with Three Extended Arms. *J Biol Chem* **282**: 24777–83.
23. Benefield D.A., Dessain S.K., Shine N., Ohi M.D., Lacy D.B. (2013) Molecular assembly of botulinum neurotoxin progenitor complexes. *Proc Natl Acad Sci* **110**: 5630–35.
24. Lee K., Gu S., Jin L., Le T.T.N., Cheng L.W., Strotmeier J., Kruel A.M., Yao G., Perry K., Rummel A., Jin R. (2013) Structure of a Bimodular Botulinum

Neurotoxin Complex Provides Insights into Its Oral Toxicity. *PLoS Pathog* **9**: e1003690.

25. Amatsu S., Sugawara Y., Matsumura T., Kitadokoro K., Fujinaga Y. (2013) Crystal Structure of Clostridium botulinum Whole Hemagglutinin Reveals a Huge Triskelion-shaped Molecular Complex. *J Biol Chem* **288**: 35617–25.
26. Niwa K., Koyama K., Inoue S. ichi, Suzuki T., Hasegawa K., Watanabe T., Ikeda T., Ohyama T. (2007) Role of nontoxic components of serotype D botulinum toxin complex in permeation through a Caco-2 cell monolayer, a model for intestinal epithelium. *FEMS Immunol Med Microbiol* **49**: 346–52.
27. Farquhar M.G., Palade G.E. (1963) Junctional complexes in various epithelia. *J Cell Biol* **17**: 375–412.
28. Tsukita S., Furuse M., Itoh M. (1996) Molecular dissection of tight junctions. *Cell Struct Funct* **21**: 381–385.
29. Inoue K., Sobhany M., Transue T.R., Oguma K., Pedersen L.C., Negishi M. (2003) Structural analysis by X-ray crystallography and calorimetry of a haemagglutinin component (HA1) of the progenitor toxin from Clostridium botulinum. *Microbiology* **149**: 3361–70.
30. Yamashita S., Yoshida H., Uchiyama N., Nakakita Y., Nakakita S. ichi, Tonozuka T., Oguma K., Nishikawa A., Kamitori S. (2012) Carbohydrate recognition mechanism of HA70 from Clostridium botulinum deduced from X-ray structures in complexes with sialylated oligosaccharides. *FEBS Lett* **586**: 2404–10.
31. Lee K., Lam K.H., Kruel A.M., Perry K., Rummel A., Jin R. (2014) High-resolution crystal structure of HA33 of botulinum neurotoxin type B progenitor toxin complex. *Biochem Biophys Res Commun* **446**: 568–73.

32. Leppanen A., Stowell S., Blixt O., Cummings R.D. (2005) Dimeric Galectin-1 Binds with High Affinity to α2,3-Sialylated and Non-sialylated Terminal N-Acetyllactosamine Units on Surface-bound Extended Glycans. *J Biol Chem* **280**: 5549–62.

33. Connaris H., Crocker P.R., Taylor G.L. (2009) Enhancing the Receptor Affinity of the Sialic Acid-binding Domain of Vibrio cholerae Sialidase through Multivalency. *J Biol Chem* **284**: 7339–51.

34. Jobling M.G., Yang Z., Kam W.R., Lencer W.I., Holmes R.K. (2012) A Single Native Ganglioside GM1-Binding Site Is Sufficient for Cholera Toxin To Bind to Cells and Complete the Intoxication Pathway. *mBio* **3**: e00401-12.

35. Ito H., Sagane Y., Miyata K., Inui K., Matsuo T., Horiuchi R., Ikeda T., Suzuki T., Hasegawa K., Kouguchi H., Oguma K., Niwa K., Ohyama T., Watanabe T. (2011) HA-33 facilitates transport of the serotype D botulinum toxin across a rat intestinal epithelial cell monolayer. *FEMS Immunol Med Microbiol* **61**: 323–31.

36. Kametani Y., Takeichi M. (2007) Basal-to-apical cadherin flow at cell junctions. *Nat Cell Biol* **9**: 92–98.

37. Woichansky I., Beretta C.A., Berns N., Riechmann V. (2016) Three mechanisms control E-cadherin localization to the zonula adherens. *Nat Commun* **7**: 10834.

38. DeLano W.L. *The PyMOL Molecular Graphics System*, Schrödinger LLC, [online] https://www.pymol.org/citing (Accessed July 14, 2017)

39. Pettersen E.F., Goddard T.D., Huang C.C., Couch G.S., Greenblatt D.M., Meng E.C., Ferrin T.E. (2004) UCSF Chimera—A visualization system for exploratory research and analysis. *J Comput Chem* **25**: 1605–12.29.

Figure Legends

Figure 1. Molecular composition of full length-HA (FL-HA) and mini-HA.

(**a**) Reconstituted L-PTC (left panel) and protomer of HA (right panel) are represented by mesh and cartoon style (EMBD ID: 3724, PDB ID: 3V0A and 3WIN) (7, 24, 25). The figures were generated by PyMOL (38) and UCSF Chimera (39) (**b**) Schematic models of FL-HA and mini-HA. FL-HA is composed of HA1, HA2, and full-length HA3 (HA3-FL; aa 19-626) and mini-HA is composed of HA1, HA2, and HA3-mini (aa 380-626). N-terminal deletion of HA3-FL was introduced based on N-terminal sequencing of HA proteins produced by *C. botulinum* (5). (**c**) A part of FL-HA and mini-HA are represented by surface and ribbon style, respectively. N286 of HA1 (red), R528 (blue) and K607 (black) of HA3 are represented by sphere style and indicated by labeled arrows.

Figure 2. Size-exclusion chromatography.

(**a**) The reconstituted and purified mini-HA was subjected to size-exclusion chromatography (SEC), and fractions in green- and red-filled areas were collected as dimers and monomers, respectively. Arrows show dimer and monomer peaks. (**b**) FL-HA (blue), a dimer fraction of mini-HA (D, green) and a monomer fraction of mini-HA (M, red) were subjected to SEC. The retention volumes of standard proteins are indicated above with their molecular weight.

Figure 3. Transepithelial resistance assay with Caco-2 cells.

Caco-2 cells grown on Transwell chambers were treated with 51 nM of protomer of HAs (17 nM FL-HA, blue line; 25.5 nM dimer fraction mini-HA, green line; 51 nM

monomer fraction of mini-HA, red line), 102 nM of protomer of dimer fraction of mini-HA (2x, green dash) and 255 nM of monomer fraction of mini-HA (5x, red dash), from the basolateral side. TER was measured up to 24 hr post-addition. Values are means ± S.E. of triplicate wells.

Figure 4. Interaction between HAs and E-cadherin.

Direct interactions between HAs and un-immobilized/immobilized E-cadherin EC1-5-His, which was expressed in HEK293 cells and purified, are shown by pull-down assay (**a**) and sandwich ELISA (**b**), respectively. (**a**) The pull-down samples were detected by Western blotting analysis with an ECCD-2 antibody against E-cadherin. HA proteins on a PVDF membrane were stained with Coomassie brilliant blue (CBB). (**b**) E-cadherin EC1-5-His was captured on an anti-His tag antibody-coated plate. Then, HAs were added to the plate and the bound HAs were detected by ELISA with polyclonal antibody against FLAG-tag. Values are means ± S.E. of triplicate wells. $^{**}P < 0.01$; by unpaired, two-tailed *t*-test.

Figure 5. Attachment of HAs to the basolateral surface of Caco-2 cells.

(**a**) 51 nM of protomer of HAs was added to the basolateral side of Caco-2 cells grown in Transwell chambers, and monolayers were incubated for 40 min at 4°C. After fixation with 4% PFA, HAs that attached to the basolateral cell surface were detected by cell-ELISA with M2 antibody against FLAG tag. Values are means ± S.E. of triplicate wells. ns: not significant; $^{*}P < 0.05$, $^{**}P < 0.01$; by unpaired, two-tailed *t*-test. (**b**) Confocal microscopy visualization of HAs that attached to the

basal surface of Caco-2 cells. Monolayers were stained with M2 antibody against FLAG tag.

Figure 6. Pulse-chase analysis with HA-Alexa568.

(**a-c**) After Caco-2 cells grown in the Transwell chamber were incubated with 153 nM of protomer of Alexa568-labeled HAs (red) from the basolateral side for 40 min at 4°C (**a**), the cells were further incubated with 153 nM of protomer of non-labeled HAs from the same side at 37°C for 10 min (**b**) or 20 min (**c**). Monolayers were stained with DECMA-1 antibody against E-cadherin (green) and ZO1-1A12 antibody against ZO-1 (blue). Images were acquired in the x-z plane (**a**, **b**) and x-y plane at the middle of the cell height (**c**). Scale bars: 5 μm (**a, b**) or 10 μm (**c**).

Supplemental Figure 1. Size-exclusion chromatography of HA proteins.

(**a**) The purified HA subcomponent protein was subjected to SEC. The retention volumes of standard proteins are indicated above with their molecular weight. The peaks with a single asterisk showed no protein band on SDS-PAGE. (**b, c**) After incubation at 37°C for 0 hr (deep purple), 6 hr (light blue), and 24 hr (light green), a dimer fraction (**b**) and a monomer fraction (**c**) of mini-HA were subjected to SEC. The peaks with double asterisks contain HA1 and HA2.

List of Abbreviations

aa, amino acid; AJ, adherence junction; BoNT, botulinum neurotoxin; CBB, Coomasie brilliant blue; EC, ectodomain; ELISA, enzyme linked immunosorbent assay; FL, full-length; HA, hemagglutinin; HRP, horseradish-peroxidase; ITC, isothermal titration calorimetry; K_d, dissociation constant; NAP, neurotoxin-associated protein; NTNHA, non-toxic non-hemagglutinin; PBS, phosphate-buffered saline; PFA, paraformaldehyde; PTC, progenitor toxin complex; SEC, size-exclusion chromatography; TBS, Tris-buffered saline; TER, transepithelial electrical resistance; TJ, tight junction; WT, wild-type.

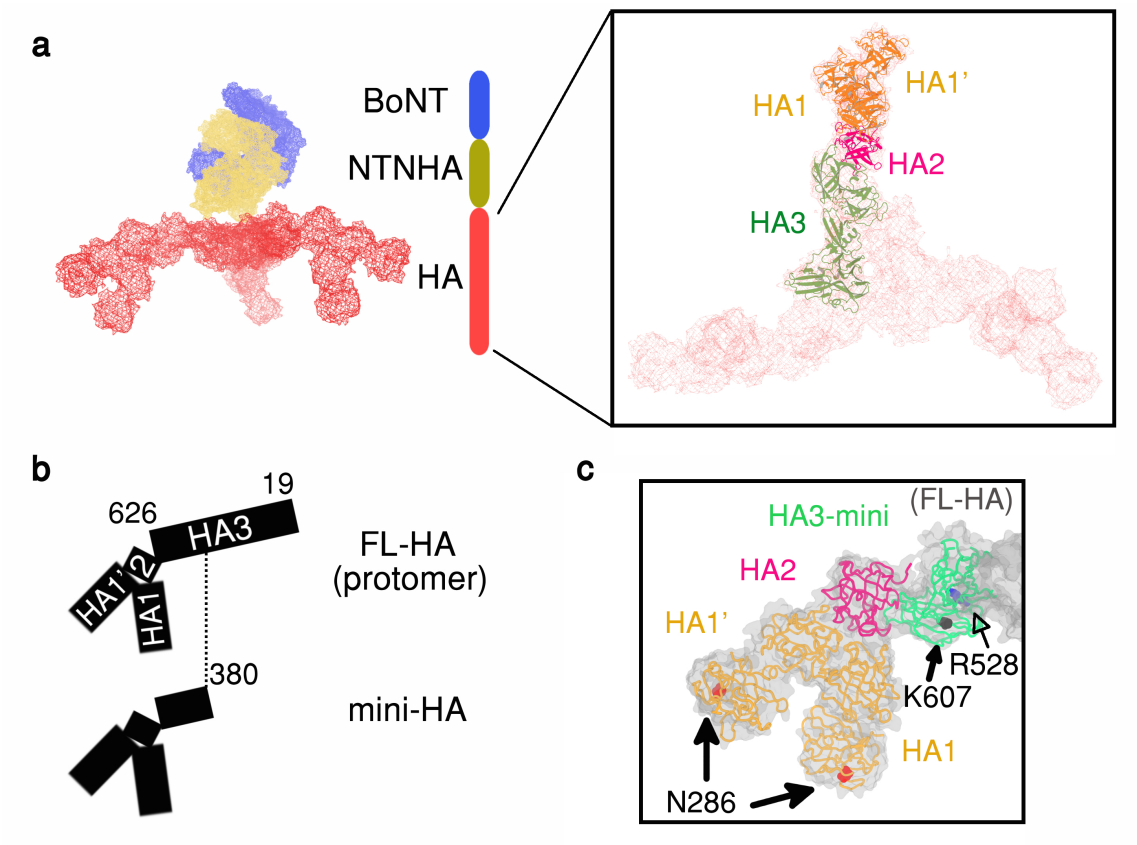

Figure 1. Molecular composition of full length-HA (FL-HA) and mini-HA.

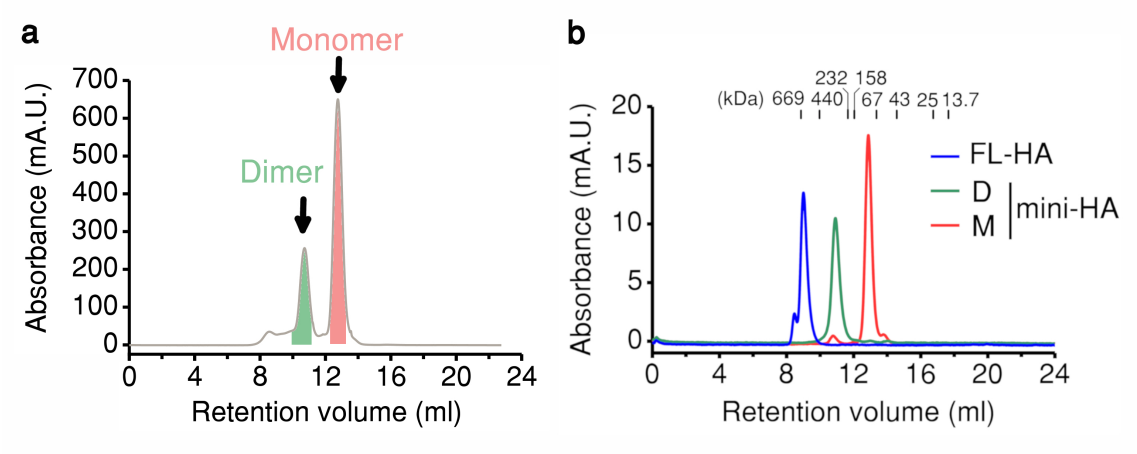

Figure 2. Size-exclusion chromatography.

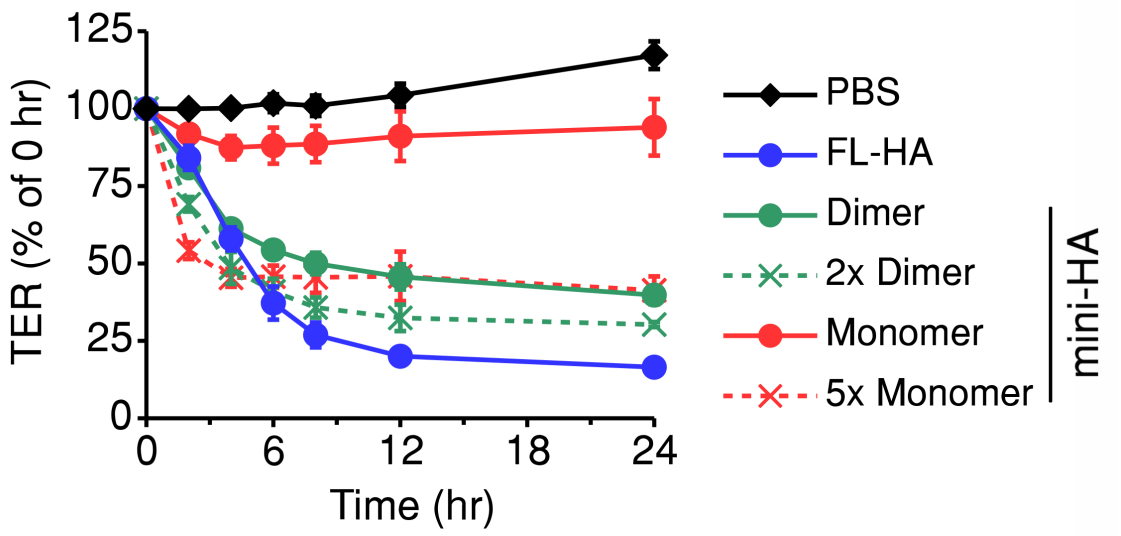

Figure 3. Transepithelial resistance assay with Caco-2 cells.

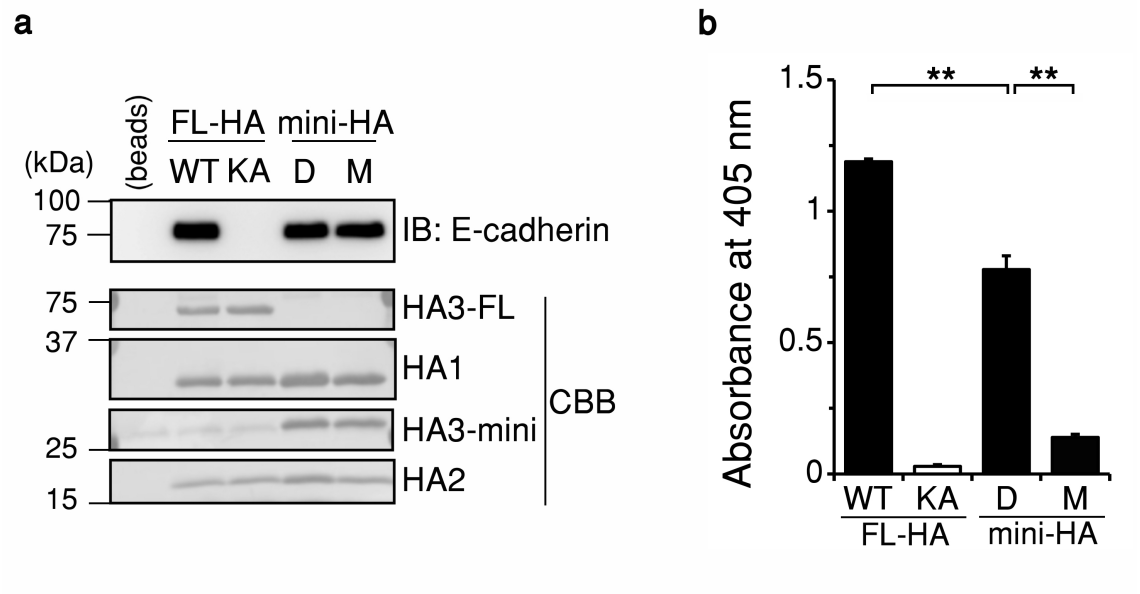

Figure 4. Interaction between HAs and E-cadherin.

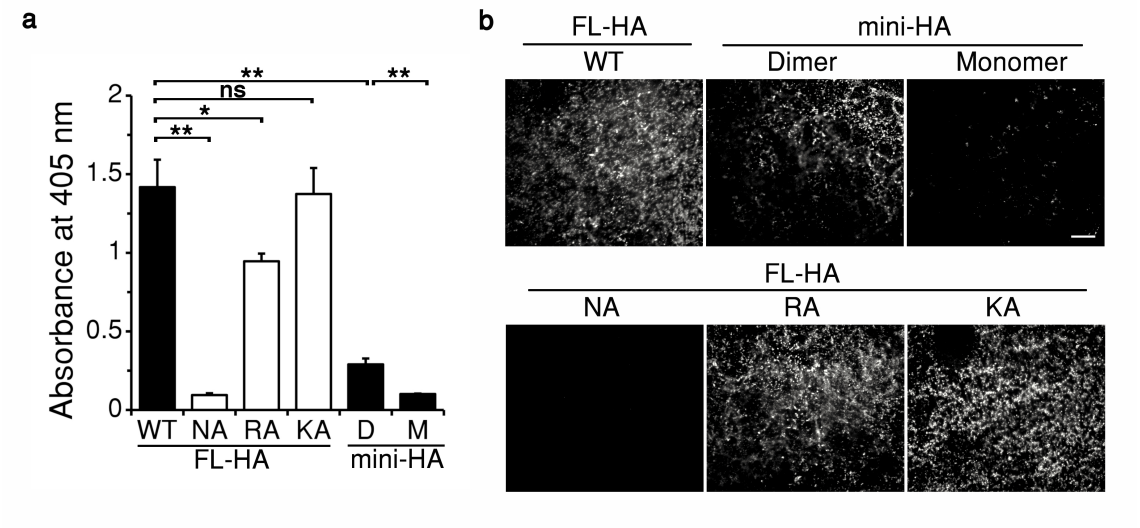

Figure 5. Attachment of HAs to the basolateral surface of Caco-2 cells.

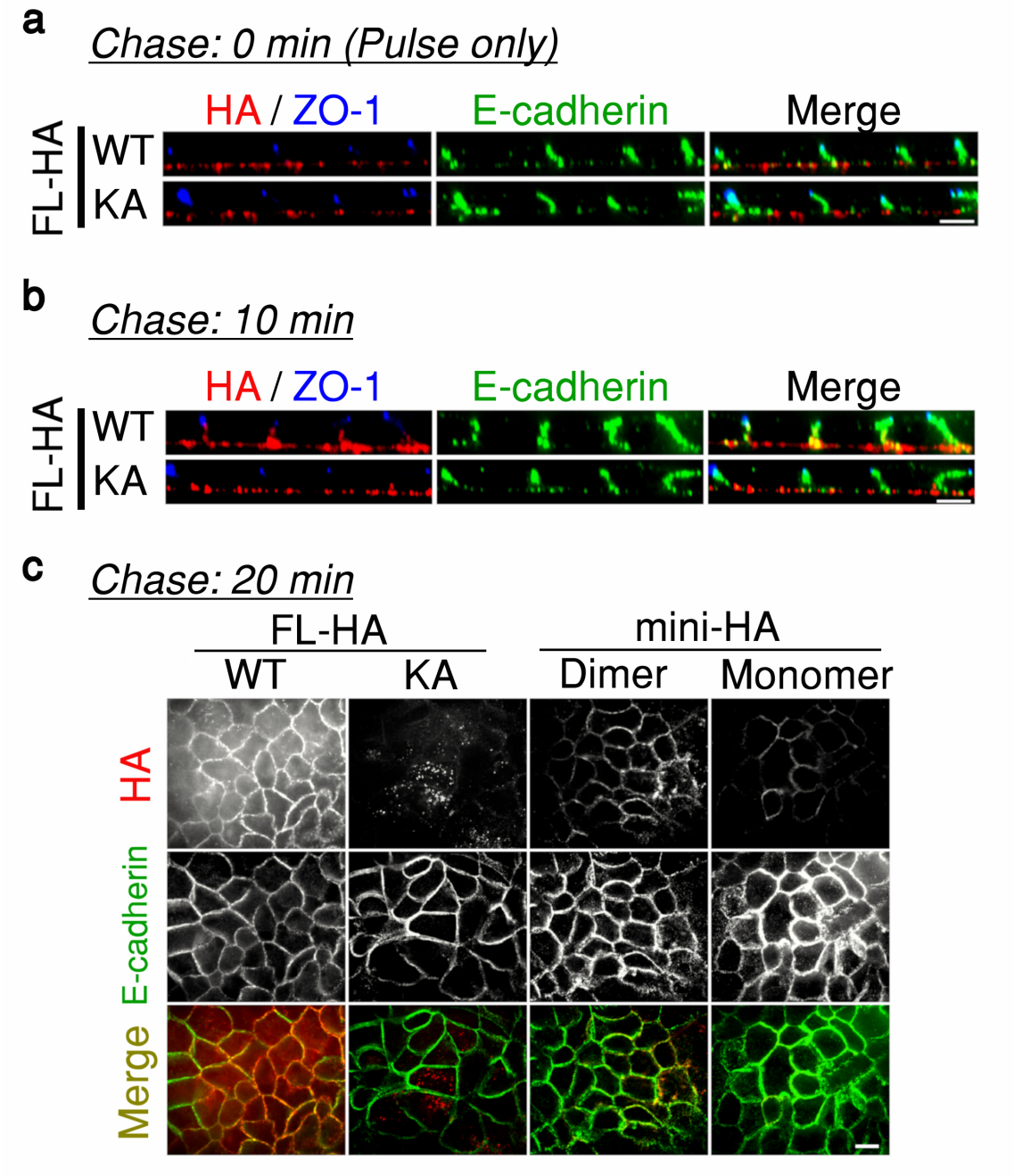

Figure 6. Pulse-chase analysis with HA-Alexa568.

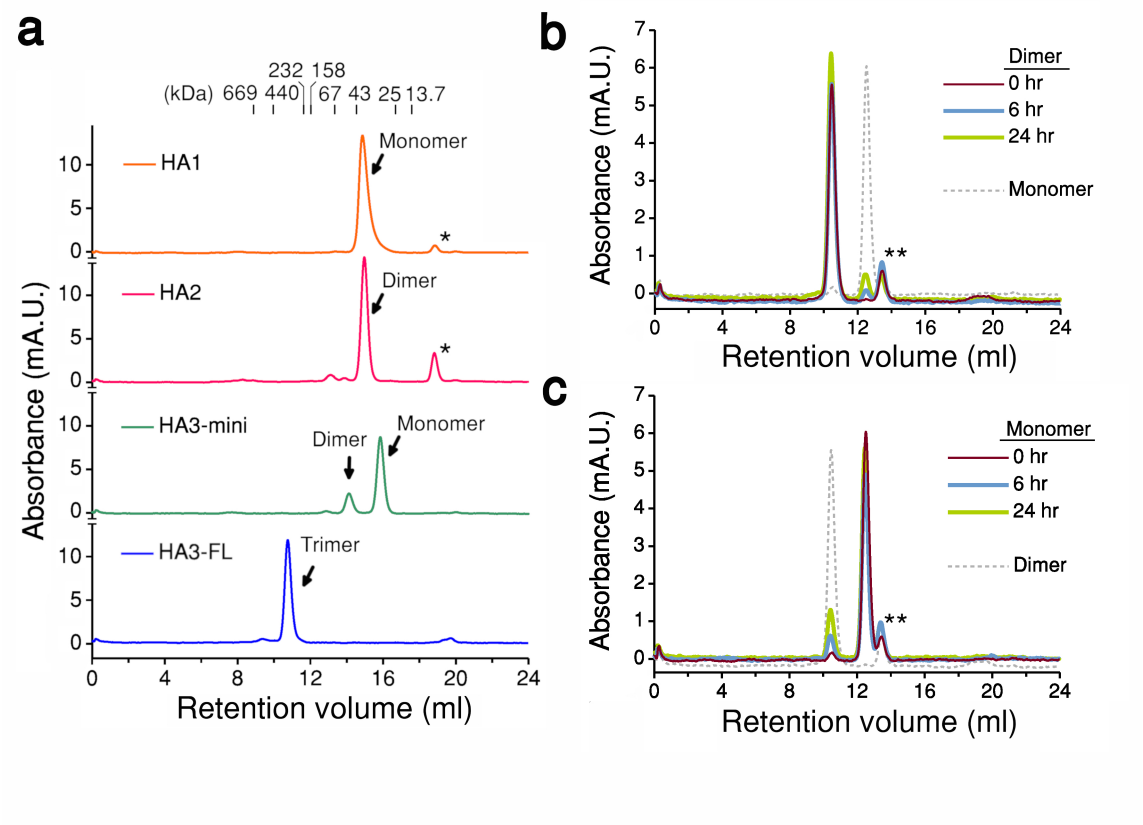

Supplemental Figure 1. Size-exclusion chromatography of HA proteins.